Journal of Materials Science: Materials in Electronics (2019) 30:19691–19702
https://doi.org/10.1007/s10854-019-02320-x

Simple synthesis and characterization of $Li_{0.5}Fe_{2.5}O_4$, $LiMg_{0.5}Fe_2O_4$ and $LiNi_{0.5}Fe_2O_4$, and investigation of their photocatalytic and anticancer properties on hela cells line

Faezeh Gandomi[1] · Seyed Mahdi Peymani-Motlagh[2,3] · Mojtaba Rostami[4] · Ali Sobhani-Nasab[5,6] · Mahdi Fasihi-Ramandi[2] · Mohammad Eghbali-Arani[7] · Roohollah Ahmadian[2,3] · Nazila Gholipour[1] · Mehdi Rahimi-Nasrabadi[2,3] · Mohammad Reza Ganjali[8,9]

Received: 18 June 2019 / Accepted: 9 October 2019 / Published online: 19 October 2019

Abstract

In the present work, the anticancer, photocatalytic and magnetic qualities of nanocrystalline nickel or magnesium-doped nanoparticles of lithium-ferrite samples, formed through sol–gel auto-combustion process were investigated. The products were studied by FT-IR spectroscopy, scanning electron microscopy (SEM), energy dispersive X-ray (EDX) technique, X-ray diffraction (XRD), ultraviolet–visible diffuse reflectance spectroscopy (DRS), photoluminescence (PL) spectra, and vibrating sample magnetometery (VSM). XRD results showed that the nano-photocatalytic samples lithium ferrite ($Li_{0.5}Fe_{2.5}O_4$), lithium-magnesium ferrite ($LiMg_{0.5}Fe_2O_4$) and lithium-nickel ferrite ($LiNi_{0.5}Fe_2O_4$) are nano-photocatalytic samples, which are in good crystalline form. The $LiMg_{0.5}Fe_2O_4$ nano-photocatalyst showed the highest photocatalytic performance for removal of methyl orange (MO) and removed 99.9% of pollutant within 25 min under ultraviolet (UV) light irradiation. Magnetic characterization revealed that the M_r and M_s of $LiNi_{0.5}Fe_2O_4$ nano-photocatalyst decreases with doping Ni or Mg. Finally, in vitro cytotoxic effect of synthesized nanoparticles was evaluated on Hela cell line.

1 Introduction

Hazardous organic materials (carbon based compounds: e.g. methyl orange, rhodamine B, phenol, bisphenol, methylene blue, etc.) are important sources of wastewater contamination. They can be removed in wastewater contamination by the photocatalytic method of semiconductor hybrid nanophotocatalysts (e.g. $CuWO_4$/NiO, $SmVO_4$, TiO_2–graphene–$ZnFe_{2-x}Tb_xO_4$, $SrTiO_3$, $NiTiO_3$, $CdTiO_3$, $CeVO_4$, Nd_2TiO_5, $Yb_2(MoO_4)3/YbMoO_4$, $BaFe_{12}O_{19}$/$Sm_2Ti_2O_7$/Ag, Pr^{3+} ions in cobalt–nickel ferrite, etc.) [1–10]. In recent years, significant progresses have been made in the photocatalytic degradation of hazardous organic materials under UV-light ($\lambda < 387$ nm). Thus, effective utilization of UV-light is a common way for photocatalytic degradation of hazardous organic pollutants [11–13].

✉ Ali Sobhani-Nasab
Ali.sobhaninasab@gmail.com

✉ Mehdi Rahimi-Nasrabadi
Rahiminasrabadi@gmail.com

1 Students' Scientific Research Center (SSRC), Tehran University of Medical Sciences (TUMS), Tehran, Iran

2 Molecular Biology Research Center, Systems Biology and Poisoning Institute, Baqiyatallah University of Medical Sciences, Tehran, Iran

3 Faculty of Pharmacy, Baqiyatallah University of Medical Sciences, Tehran, Iran

4 Young Researchers and Elite Club, Islamic Azad University, Karaj Branch, Karaj, Iran

5 Social Determinants of Health (SDH) Research Center, Kashan University of Medical Sciences, Kashan, Iran

6 Core Research Lab, Kashan University of Medical Sciences, Kashan, Iran

7 Department of Physics, University of Kashan, Kashan, Iran

8 Center of Excellence in Electrochemistry, School of Chemistry, College of Science, University of Tehran, Tehran, Iran

9 Biosensor Research Centre, Endocrinology & Metabolism Molecular and Cellular Research Institute, Tehran University of Medical Sciences, Tehran, Iran

Spinel-phase nanocrystalline $Li_{0.5-0.5x}M_xFe_{2.5-0.5x}O_4$ (e.g. M = Mg^{2+}, Ni^{2+}, Fe^{2+}, Co^{2+}, Cd^{2+}, Zn^{2+}, Cu^{2+}, Mn^{2+}, etc.) magnetic ferrites constitute a key family of nanomaterials which are suitable for a range of applications like nanoferro fluids, nano-biomedical, nano-photocatalysts, magnetic, microwave, and gas sensing devices [14, 15].

Because $Li_{0.5}Fe_{2.5}O_4$ enjoys qualities such as having low dielectric loss, high saturation magnetization, square hysteresis loop, low cost and environmental friendliness, and being non-toxicity, it could be considered as a potential magnetic material for hybrid nanophotocatalysts [16]. The varied qualities of spinel lithium ferrites can be attributed to their ability to host the cations for a range of transition metals in their lattice. Therefore, their structural, optical, magnetic and electrical characteristics can change. New approaches, like radio-frequency inductively coupled plasma (RF-ICP), chemical hydrothermal, electrochemical, microwave or sonochemical processing, inert gas condensation, sol–gel auto-combustion, and mechanical milling have been introduced for preparing spinel ferrite nanoparticles [17–20]. A very common choice from this list has been the sol–gel auto-combustion (SGAC) approach which has been used in the synthesis of materials with different metastable structures, even at rather low temperatures, because this method yields products with great chemical homogeneity. Such method offers the possibility to manipulate physical characteristics such as particle size and shape, and pore structure in the product by varying the preparation conditions [21, 22].

On the other hand, the contemporary state of exposure to nanomaterials has attracted a great deal of attention to the evaluation of their antibacterial and nanotoxicology, and the incremental trends in the application of nanoparticles [23–25]. They increase the need for more techniques for their evaluation and analysis. It is also important to pinpoint and describe the physicochemical properties of the particles which affect their toxicity and use this information for obtaining desirable products. Herein, we report the synthesis of the Ni or Mg-doped $Li_{0.5}Fe_{2.5}O_4$ nano-crystalline magnetic ferrites using the sol–gel auto-combustion process for in vitro cytotoxicity assay and catalytic photo degradation of aqueous solution of MO under ultraviolet light irradiation.

2 Experimental section

2.1 Chemicals

Nickel nitrate hexahydrate (99%), magnesium nitrate hexahydrate (99%), ferric nitrate nanohydrate (99%), lithium nitrate (99%), Ammonia solution (25%) and citric acid monohydrate (99%) were obtained from Merck Co. and used as received. All solutions and washings were performed using deionized water (DI) prepared using a TKACo Smart-2-Pure instrument.

2.2 Preparation of Ni or Mg-doped $Li_{0.5}Fe_{2.5}O_4$ magnetic nanophotocatalysts

Nanocrystalline Ni or Mg-doped $Li_{0.5}Fe_{2.5}O_4$ magnetic nanophotocatalysts were synthesized by the simple wet chemical SGAC method. $LiNO_3$, $Fe(NO_3)_3{\cdot}9H_2O$, $Ni(NO_3)_2{\cdot}6H_2O$ and $Mg(NO_3)_2{\cdot}6H_2O$ were used as precursors to prepare $Li_{0.5}Fe_{2.5}O_4$, $LiMg_{0.5}Fe_2O_4$ and $LiNi_{0.5}Fe_2O_4$ magnetic nanophotocatalysts. The metal nitrate/citric acid monohydrate molar ratio was kept at 1:3 at room temperature. Typical preparation procedures involved dissolving $LiNO_3$, $Fe(NO_3)_3{\cdot}9H_2O$, citric acid and $Ni(NO_3)_2{\cdot}6H_2O$ or $Mg(NO_3)_2{\cdot}6H_2O$ in 100 mL of DI, with stirring 3000 rpm for 3 h to form a stable solution at normal temperature. Next liquid ammonium hydroxide was added to the solution in a drop wise manner to pH of 7 while the solution was heated at 80 °C for 60 min, to yield a transparent sol. This was heated for another 60 min at 110 °C to evaporate the water. Further increase in the temperature turned the sol to a viscous brown gel, and eventually dried gel at 100 °C for 60 min. When a certain temperature was reached, the sample ignited and the dried gel burnt to form the magnesium or nickel-substituted lithium ferrite powder. This powder was next dried and sintered for 120 min at 900 °C in a muffle furnace.

2.3 Assessment of the nano-particles

XRD phase analyses were conducted using a Philips X'pert Pro MPD with a graphite-filtered Cu Kα (k = 0.154 nm) radiation. These analyses were performed in a 2θ window ranging from 10 to 80°. Sample morphology was also studied through performing SEM tests at 30 kV on a Tescan MIRA3 FEG-SEM equipped with a Tescan MIRA3 FEG-EDAX. To perform the tests, the samples were dispersed onto a carbon tape. Fourier transform infrared spectra were recorded using a Nicolet Magna IR 550 spectrometer and the room temperature magnetic measurements were performed using a PMC Micro Mag 3900 VSM (Meghnatis Daghigh Kavir Co.) with a 1 Tesla magnet.

2.4 Photodegradation assessments

The suspensions used for the photo-degradation reaction were 500 mL of a 0.1 g/L suspension of $Li_{0.5}Fe_{2.5}O_4$, $LiMg_{0.5}Fe_2O_4$ and $LiNi_{0.5}Fe_2O_4$ nanostructure photocatalyst in a 5 mg/L MO solution as the model pollutant. The irradiation was performed using a high pressure Hg lamp (250 W, λ > 280 nm). The suspension was stirred in the absence of light until the ongoing analyses showed an equilibrium was reached (this happened after 30 min). The suspensions were subjected to UV under constant aeration. At 0, 5, 10, 15, 20

and 30 min of the onset of the irradiation, the reaction mixture was sampled and the samples were studied by UV–Vis spectrometry at the maximum absorbance (λmax = 507) of MO at 25 °C, after centrifugation. The temperature of sample was maintained at 25 °C by cooling the reactor.

2.5 Cell culture

A 549 cell line was the curtesy of the National Cell Bank of Iran. The culturing of the cells was performed using 75 cm^2 flasks, and next the cells were scraped off and centrifuged at 1100×*g* for 5 min, before being resuspended in a fresh medium and, counted by trypan blue exclusion (99% viability). The concentration of the cells was set at 10^5 cells/mL. 100 µL volumes of the suspension were transferred to the wells of a 96-well cell-culture plate (Corning, USA) containing a RPMI-1640 medium (Cambrex Bioscience), further containing L-glutamine (2 mM, Gibco), penicillin–streptomycin (100 IU/mL penicillin, 100 mg/mL streptomycin (Gibco)) and heat inactivated fetal bovine serum (Biowest) 10% (v/v). The system was stored in a humidified incubator with a 5% CO_2 atmosphere at 37 °C.

2.6 MTT assay

Different concentration of nanoparticles were added to cultured 96-well plate and 24 and 48 h after irradiation, After adding MTT solution (USB Corporation, Cleveland, USA) to the wells, the plates were incubated at 37 °C for 4 h. Next, the MTT solution was taken away and DMSO was used to dissolve the formazan crystals. The absorbance of the sample at 540 nm was measured using a 680 Microplate Reader, Bio-Rad Laboratories, Hercules, CA, USA. The viability percentage was calculated using the expression below:

AT/AC × 100

in which AT and AC represent the absorbance of the treated and control cells, respectively.

3 Results and discussions

3.1 XRD analysis

The obtained XRD analysis of the magnesium or nickel substituted lithium ferrites magnetic nanophotocatalyst samples with chemical formula of $LiMg_{0.5}Fe_2O_4$ and $LiNi_{0.5}Fe_2O_4$, respectively, calcinated at 900 °C for 2 h is illustrated in Fig. 1. The XRD results show a series of diffraction peaks at the position of 24.1°, 26.19°, 31.14°, 36.11° 44.33°, 54.66° 57.46° and 63.22° with lines (210), (211), (220), (222), (400), (422), (511) and (440) which is in good agreement with $Li_{0.5}Fe_{2.5}O_4$ with the cubic spinel-phase lattice structure [26–30].

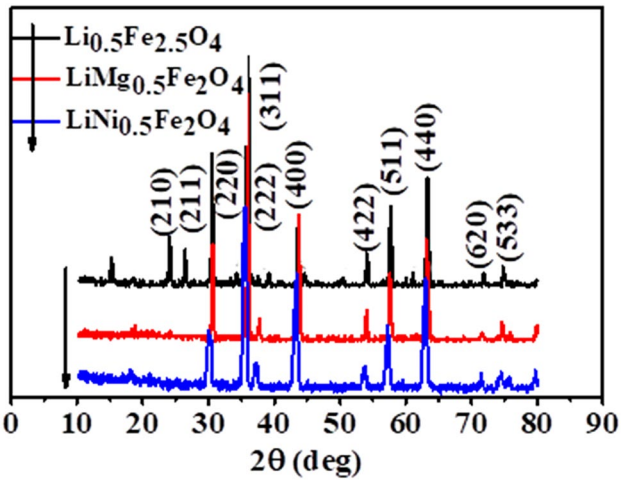

Fig. 1 XRD patterns of the $Li_{0.5}Fe_{2.5}O_4$, $LiMg_{0.5}Fe_2O_4$ and $LiNi_{0.5}Fe_2O_4$ magnetic nano-particles

The approximate size of the crystallite phases of the sample was determined using XRD-peak data and the Debye–Scherrer formula [31–38]:

$$D = \frac{k\lambda}{\beta \cos\theta}, \quad (1)$$

in which k is a constant (0.9), λ or the X-ray radiation is 0.154056 nm, β expresses a corrected band broadening (full-width at half-maximum) obtained after subtracting the instrumental broadening, and θ represents Bragg's angle. The average values of the crystallite sizes of the samples sintered at 900 °C were calculated via the Debye–Scherrer equation applied to the marked peaks, and the crystal sizes were 37 ± 0.2 nm, 45 ± 0.2 nm and 41 ± 0.2 nm for $Li_{0.5}Fe_{2.5}O_4$, $LiMg_{0.5}Fe_2O_4$ and $LiNi_{0.5}Fe_2O_4$, respectively.

3.2 SEM and EDX tests

Surface morphology and composition of magnetic nanoparticles was investigated by SEM analysis. Figure 2 shows TEM, SEM and EDS images of the (a) $Li_{0.5}Fe_{2.5}O_4$, (b) $LiMg_{0.5}Fe_2O_4$ and (c) $LiNi_{0.5}Fe_2O_4$ magnetic nanoparticles prepared by the sol–gel method. TEM and SEM image show that all the magnetic nanoparticles display approximately spherical shape. It is found that the average diameter of the nanoparticles increased with doping Mg or Ni on to the $Li_{0.5}Fe_{2.5}O_4$, and average diameter size were in the range of about from 90 to 127 nm, in the case of the un-doped

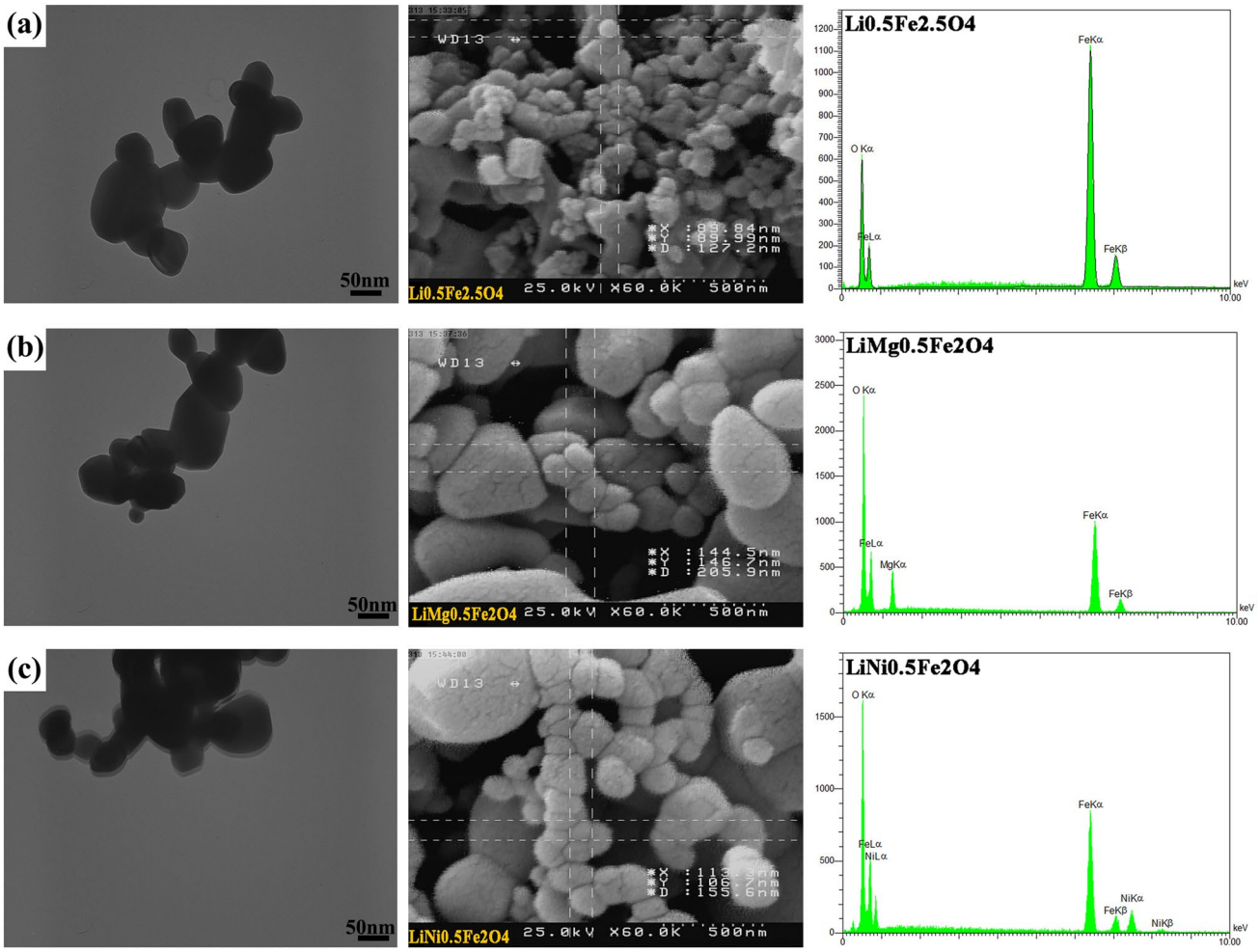

Fig. 2 TEM, SEM pictures and EDX spectra of the **a** $Li_{0.5}Fe_{2.5}O_4$, **b** $LiMg_{0.5}Fe_2O_4$ and **c** $LiNi_{0.5}Fe_2O_4$ magnetic nano-particles

and ~ 140–205 nm for the magnesium-doped $Li_{0.5}Fe_{2.5}O_4$ and ~ 113 – 155 nm for Ni-doped $Li_{0.5}Fe_{2.5}O_4$ samples. In the case of pure $Li_{0.5}Fe_{2.5}O_4$ samples, the EDX spectra included Li, Fe and O peaks, and in the case of the magnetic Ni or Mg-doped $Li_{0.5}Fe_{2.5}O_4$ samples, Fe, Mg, Li, Ni and O peaks could be observed.

3.3 FT-IR spectroscopy

The infrared spectroscopy results obtained for $Li_{0.5}Fe_{2.5}O_4$, $LiMg_{0.5}Fe_2O_4$ and $LiNi_{0.5}Fe_2O_4$ can be viewed in Fig. 3. The absorption bands around 580.7, 590.7 and 599.0 cm^{-1} correspond to the presence of metal oxide (Fe–O). Furthermore, the bands at 3417 and 1629 cm^{-1} reflect the stretching/bending of the hydroxyl groups [39]. However, the $Li_{0.5}Fe_{2.5}O_4$ nanoparticles prepared using citric acid had spinel (P_4 332 space group) absorption bands at 466.7 and 544.7 cm^{-1} [40]. Doping the product with Mg or Ni enhanced the wavenumber, because of the replacement of the smaller Fe^{3+} (63 pm) ions with Mg^{2+} (71 pm) and Ni^{2+} (83 pm) [41].

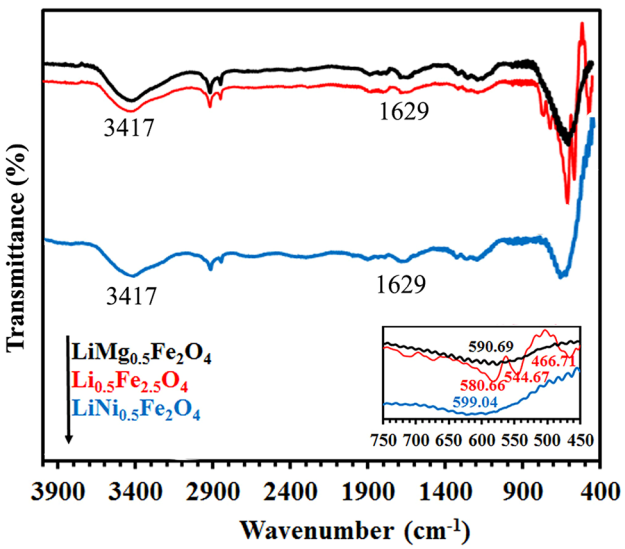

Fig. 3 FT-IR spectra of the $Li_{0.5}Fe_{2.5}O_4$, $LiMg_{0.5}Fe_2O_4$ and $LiNi_{0.5}Fe_2O_4$ magnetic nano-particles

3.4 Magnetic characterization

The Magnetic hysteresis plots of $Li_{0.5}Fe_{2.5}O_4$, $LiMg_{0.5}Fe_2O_4$ and $LiNi_{0.5}Fe_2O_4$ magnetic nanophotocatalysts samples are shown in Fig. 4. The $Li_{0.5}Fe_{2.5}O_4$ nanophotocatalysts exhibits higher M_s and M_r than Mg or Ni-doped $Li_{0.5}Fe_{2.5}O_4$. It is clear that the M_s and M_r decrease with doping Mg or Ni. Maximum Ms, M_r and H_c values were 57.757 emu/g, 17.420 emu/g and of 100.783 Oe. The results of the magnetic parameters measurement as remanence magnetization (M_r), coercivity (H_c) and saturation magnetization (M_s) values are summarized in Table 1. M_r usually depends on M_s, Thus by decreasing the Bohr magnetization in the prepared samples, saturation magnetizations (M_s) and remanent magnetization M_r decrease. But H_c determined by a lot of extrinsic factors such as crystal size, single-domain or multi-domain, anisotropy, and etc. that is strongly influenced by microstructure of samples in the processing procedures. However, H_c of the samples are almost identical and this indicate that these factors are almost same in all samples.

3.5 Photoluminescence (PL) evaluations

Figure 5 shows the photoluminescence spectra obtained for $Li_{0.5}Fe_{2.5}O_4$, $LiMg_{0.5}Fe_2O_4$ and $LiNi_{0.5}Fe_2O_4$ magnetic nanophotocatalyst samples. PL spectra of Ni or Mg-doped $Li_{0.5}Fe_{2.5}O_4$ were acquired in order to study the defects and effects of impurity on the system. To this end, the samples were excited at 533–563 nm. All samples showed the near-band-edge (NBE) bands characteristic of $Li_{0.5}Fe_{2.5}O_4$ and magnesium- or nickel doped $Li_{0.5}Fe_{2.5}O_4$ at about 565, 533 and 545 nm. Moreover, a wider emission was observed in all cases. This was attributed to the recombination of photogenerated holes with electrons which were deeply trapped in oxygen vacancies [42]. Doping was found to decrease the overall intensity of the peaks of both samples, due to the emergence of electronic levels with energies between those of the conduction and valence bands as a result of increased defects [43]. Hence the charge separation efficiency and photocatalytic activity are expected to have an inverse relationship of $LiMg_{0.5}Fe_2O_4 > LiNi_{0.5}Fe_2O_4 > Li_{0.5}Fe_{2.5}O_4$ [44].

Table 1 Magnetic parameters of the nanophotocatalysts samples

Sample	MS (emu/g)	Mr (emu/g)	HC (kQe)
$Li_{0.5}Fe_{2.5}O_4$	57.757	17.42	100
$LiMg_{0.5}Fe_2O_4$	26.44	12.646	90.342
$LiNi_{0.5}Fe_2O_4$	26.131	6.763	100.783

3.6 UV–visible Diffuse reflectance spectroscopy (UV–Vis DRS) experiments

UV–visible diffuse reflectance spectra of the $Li_{0.5}Fe_{2.5}O_4$, $LiMg_{0.5}Fe_2O_4$ and $LiNi_{0.5}Fe_2O_4$ magnetic nanophotocatalyst samples are illustrated with maximum absorption around 370, 388 and 405 nm, respectively. Also, Fig. 6a, b clearly indicate a drop in the band gap energy of the doped samples as opposed to pristine $Li_{0.5}Fe_{2.5}O_4$, which illustrates a considerable red shift and increase in the absorption in the case of Mg and Ni-doped $Li_{0.5}Fe_{2.5}O_4$ magnetic nanophotocatalysts compared to $Li_{0.5}Fe_{2.5}O_4$ (Table 2). The direct optical band gap energies (E_g) of the magnetic nanophotocatalyst samples were calculated according to the Tauc relationship as given below [45]:

$$\alpha h\nu = B\,(h\nu - E_g)^2 \quad (2)$$

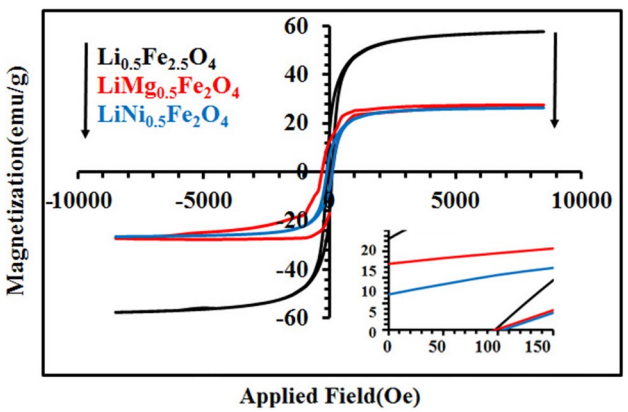

Fig. 4 Magnetic hysteresis loops (or the M–H curves) of the $Li_{0.5}Fe_{2.5}O_4$, $LiMg_{0.5}Fe_2O_4$ and $LiNi_{0.5}Fe_2O_4$ magnetic nano-particles

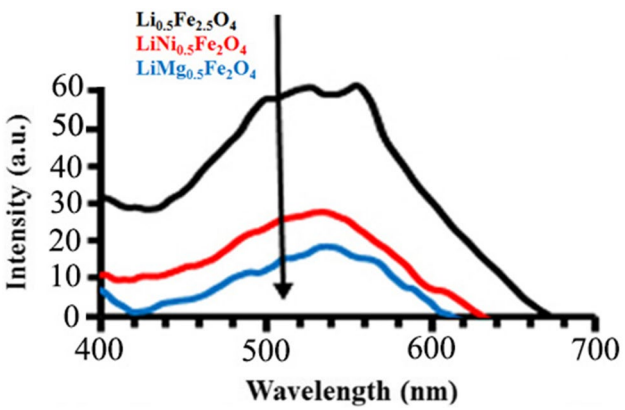

Fig. 5 PL spectra of the $Li_{0.5}Fe_{2.5}O_4$, $LiMg_{0.5}Fe_2O_4$ and $LiNi_{0.5}Fe_2O_4$ magnetic nano-particles

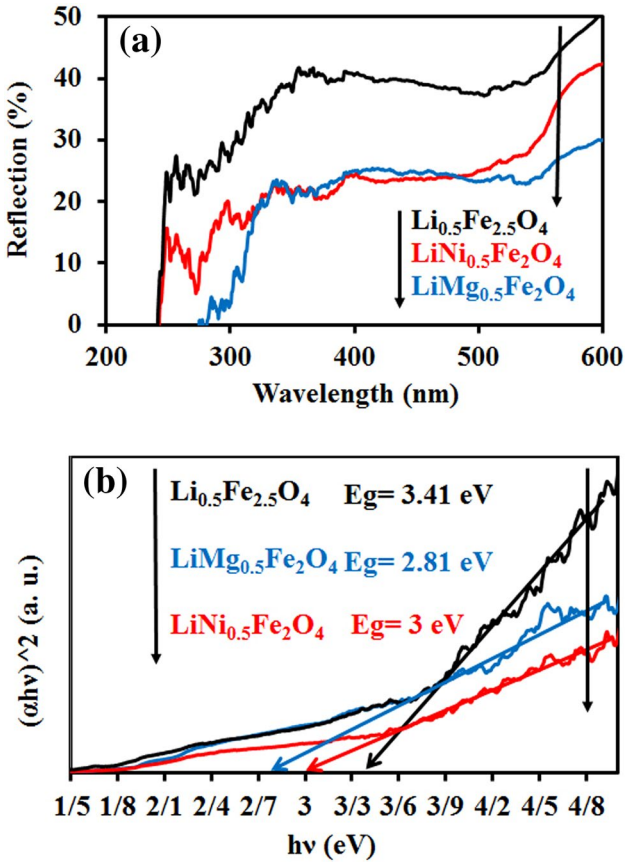

Fig. 6 $Li_{0.5}Fe_{2.5}O_4$, $LiMg_{0.5}Fe_2O_4$ and $LiNi_{0.5}Fe_2O_4$ magnetic nanoparticles: **a** UV–Vis spectra, and **b** Tauc plot pattern (band gap energy)

3.7 Photocatalytic studies of nanophotocatalyst samples

UV–vis absorption spectra of MO dye after the photodegradation under UV light in the presence of the $Li_{0.5}Fe_{2.5}O_4$ (95%), $LiMg_{0.5}Fe_2O_4$ (98.04%) and LiNi0.5Fe_2O_4 (99.09%) magnetic nanophotocatalyst samples are illustrated in Fig. 7. The removal of MO dye by Mg or Ni-doped $Li_{0.5}Fe_{2.5}O_4$, were higher as opposed to $Li_{0.5}Fe_{2.5}O_4$. The p–d spin exchange interaction between the localized f electrons of Ni or Mg doped into $Li_{0.5}Fe_{2.5}O_4$ surrounding and the band electrons leads to narrowing. Meanwhile, pedex-change and the sed interactions give rise to a positive and a negative correction to the valence band energies and the conduction band, respectively. They happen due to reduce in band gap energy. Therefore different parameters such as strain, lattice distortion and impurity change its band gap value.

Effect of irradiation time and kinetic studies on the photodegradation MO dye in the presence of the $Li_{0.5}Fe_{2.5}O_4$, $LiMg_{0.5}Fe_2O_4$ and $LiNi_{0.5}Fe_2O_4$ magnetic nanophotocatalyst samples are illustrated in Fig. 8. Photocatalytic reactions involving the application of magnetic nano-photocatalysts fit the Langmuir–Hinshelwood model [46]. In the present case the reaction involving the magnetic nanophotocatalyst samples and UV irradiation is a pseudo 1st order reaction. The kinetics of such reactions are expressed by:

$$r = dc/dt = -kC \quad (3)$$

Integrating this equation from $C = C_0$ at $t = 0$ (C_0 is the initial bulk concentration of MO and t: reaction time) yields:

$$\ln(C/C_0) = -kt \quad (4)$$

k is the apparent rate constant, C_0 is the bulk concentration of MO before the reaction, and C is the MO concentration at any instant t after the onset of the irradiation.

Today, considering the excellent performance of different nanomaterials in photocatalyst, many scientists have focused on this field [35, 47–53]. Figure 9a, b shows the performance of magnetic nanophotocatalyst samples towards MO degradation under UV irradiation. In comparison with un doped $Li_{0.5}Fe_{2.5}O_4$, Mg or Ni-doping improves the photoactivity of $Li_{0.5}Fe_{2.5}O_4$, principally because Mg^{2+} and Ni^{2+} can act as both electron–hole (e^-–h^+) traps to enhance lifetimes of e^-–h^+ pairs [44]. The magnetic Mg-doped $Li_{0.5}Fe_{2.5}O_4$ nanophotocatalysts had outstanding photocatalytic activity for the UV induced degradation of MO at $\lambda < 387$ nm. The first event after the irradiation of the reaction dispersion containing Ni or Mg-doped $Li_{0.5}Fe_{2.5}O_4$ includes the formation of e^-–h^+ pairs, which oxidizes MO. MO may also be oxidized by reactive oxygen species active sites such as OH· and $O_2^{\cdot-}$ radicals formed on the illuminated Ni or Mg-doped $Li_{0.5}Fe_{2.5}O_4$ surface [54].

Table 2 Optical and crystal size parameters of the nanophotocatalysts samples

Sample no.	Debye–Scherrer crystallite size (nm)	Band edge (nm)	Maximum absorption	Maximum emission
$Li_{0.5}Fe_{2.5}O_4$	37	3.41	370	563
$LiMg_{0.5}Fe_2O_4$	45	2.81	388	533
$LiNi_{0.5}Fe_2O_4$	41	3	405	546

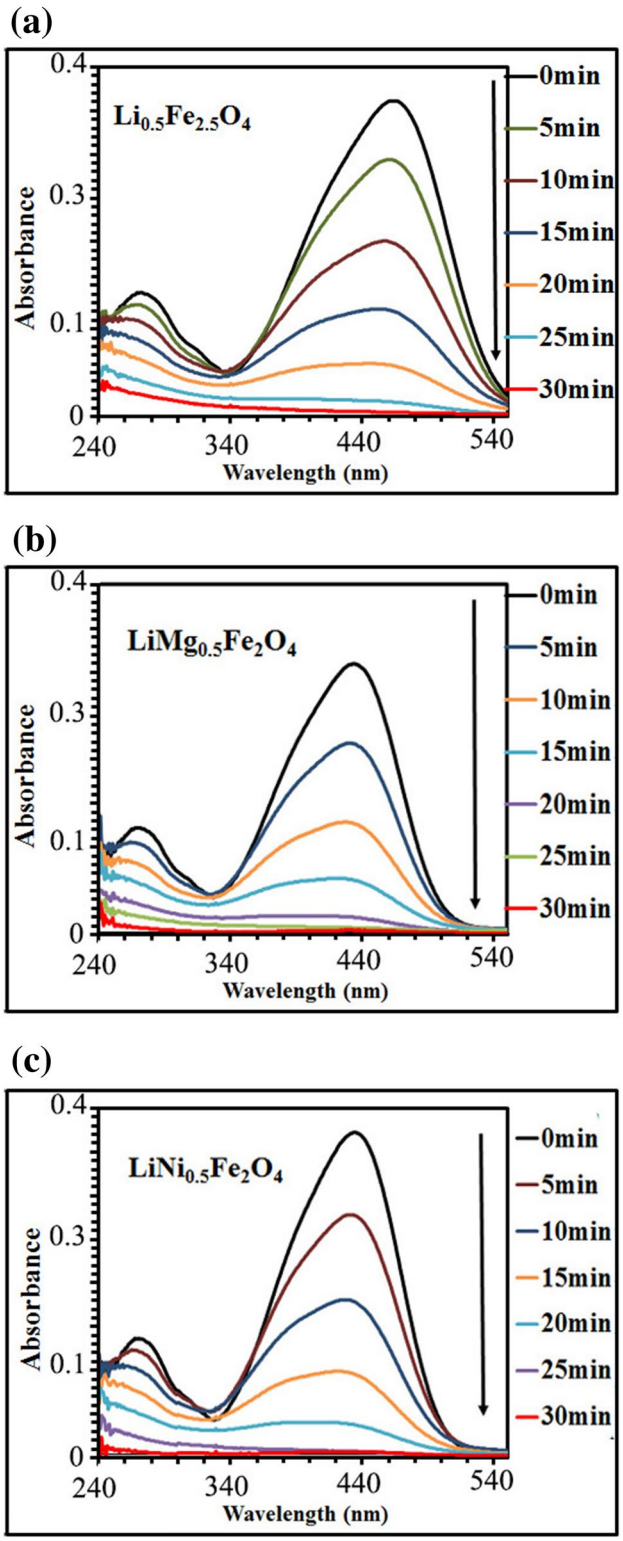

Fig. 7 UV–Vis absorbance spectrum of MO at different time intervals on irradiation using 0.1 g/L, of the $Li_{0.5}Fe_{2.5}O_4$, $LiMg_{0.5}Fe_2O_4$ and $LiNi_{0.5}Fe_2O_4$ magnetic photocatalysts

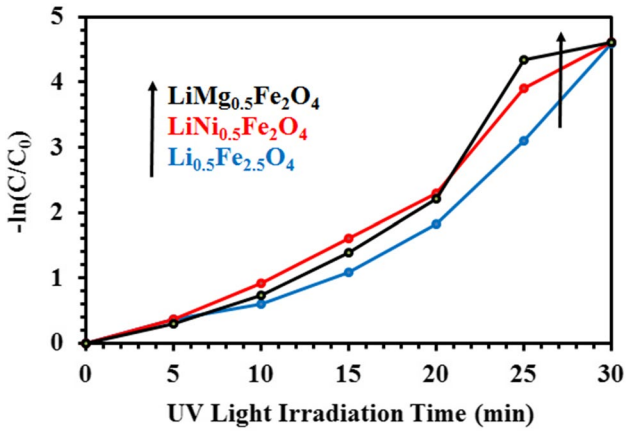

Fig. 8 Photocatalytic destruction of the $Li_{0.5}Fe_{2.5}O_4$, $LiMg_{0.5}Fe_2O_4$ and $LiNi_{0.5}Fe_2O_4$ magnetic photocatalysts (pseudo first order kinetics)

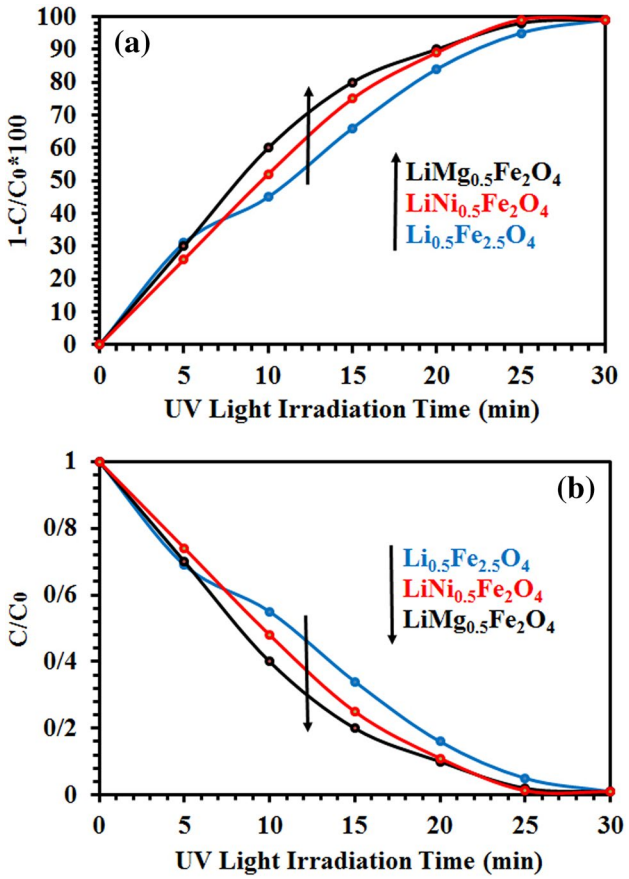

Fig. 9 **a**, **b** Photocatalytic destruction of methyl orange solution under UV irradiation of the $Li_{0.5}Fe_{2.5}O_4$, $LiMg_{0.5}Fe_2O_4$ and $LiNi_{0.5}Fe_2O_4$ magnetic photocatalysts. The photocatalytic reaction can be expressed as follows (i to v). (i) M = Mg or Ni-doped $Li_{0.5}Fe_{2.5}O_4 + h\nu \rightarrow$ Mg or Ni-doped $Li_{0.5}Fe_{2.5}O_4$ $(h^+ + e^-)$. (ii) $M^{3+} + e^- \rightarrow M^{2+}$. (iii) $M^{2+} + O_2 \rightarrow M^{3+} + O_2{\cdot}^-$. (iv) $M^{2+} + h^+ \rightarrow M^{3+}$. (v) $H_2O + h^+ \rightarrow HO\cdot + H^+$. (vi) $O_2 + e^- \rightarrow O_2{\cdot}^-$. (vii) $H^+ + O_2{\cdot}^- \rightarrow 2HO\cdot$. (viii) $\cdot OH + MO \rightarrow CO_2 + H_2O +$ Intermediate products

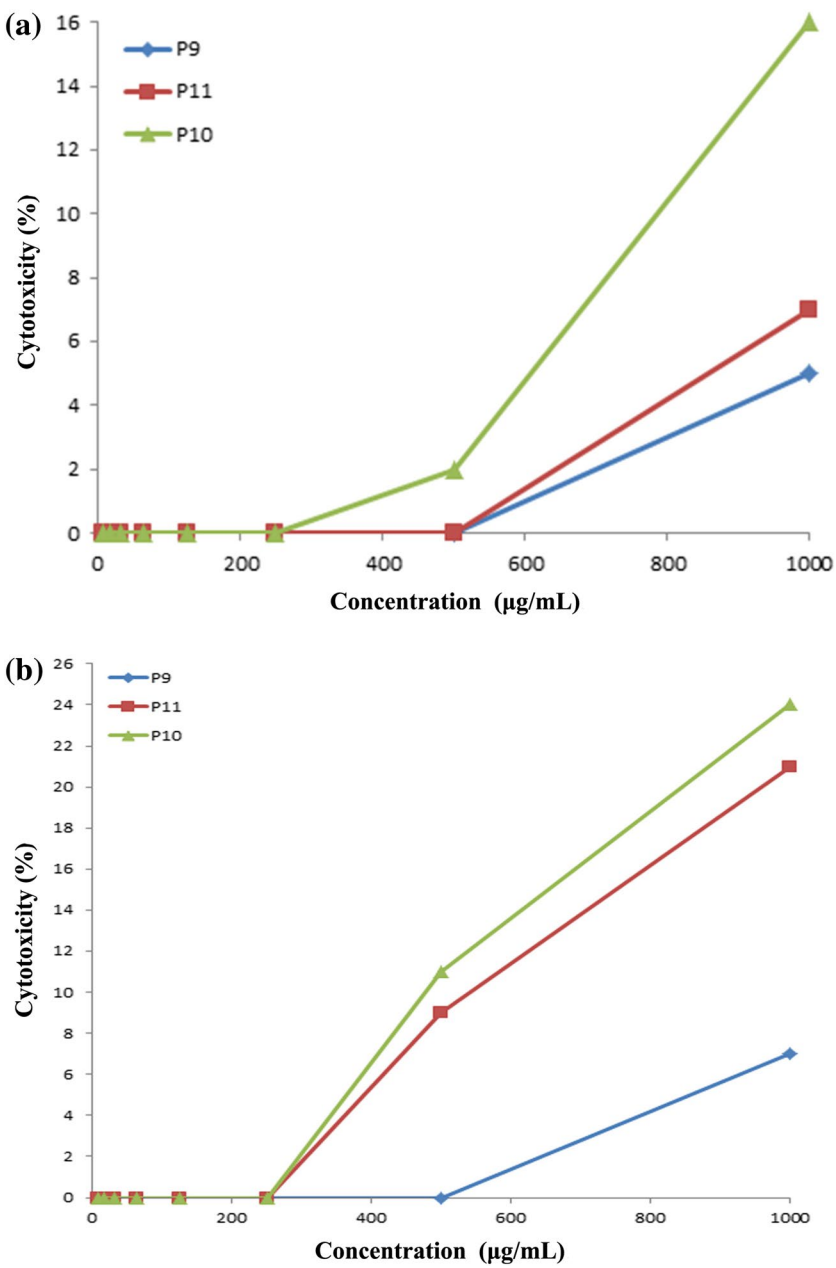

Fig. 10 Anticancer effect of the nanoparticles on hela cell after (**a**) 24 h and (**b**) 48 h

3.8 Cytotoxicity of nanoparticles

Cytotoxic effect of different concentrations of nanoparticles from 10 to 1250 µg/mL on hela cell line was considered with MTT assay. The cytotoxicity of prepared nanoparticle against the cell that was observed after 24 and 48 h treatment which are presented in Fig. 10a, b. Based on these results, after 24 h of cell treatment using nanoparticles, $Li_{0.5}Fe_{2.5}O_4$ and $LiNi_{0.5}Fe_2O_4$ nanoparticles did not show any toxicity up to a concentration of 500 µg/mL. The $LiMg_{0.5}Fe_2O_4$ nanoparticle in this concentration killed only 2% of the cells after 24 h and any toxicity was not observed

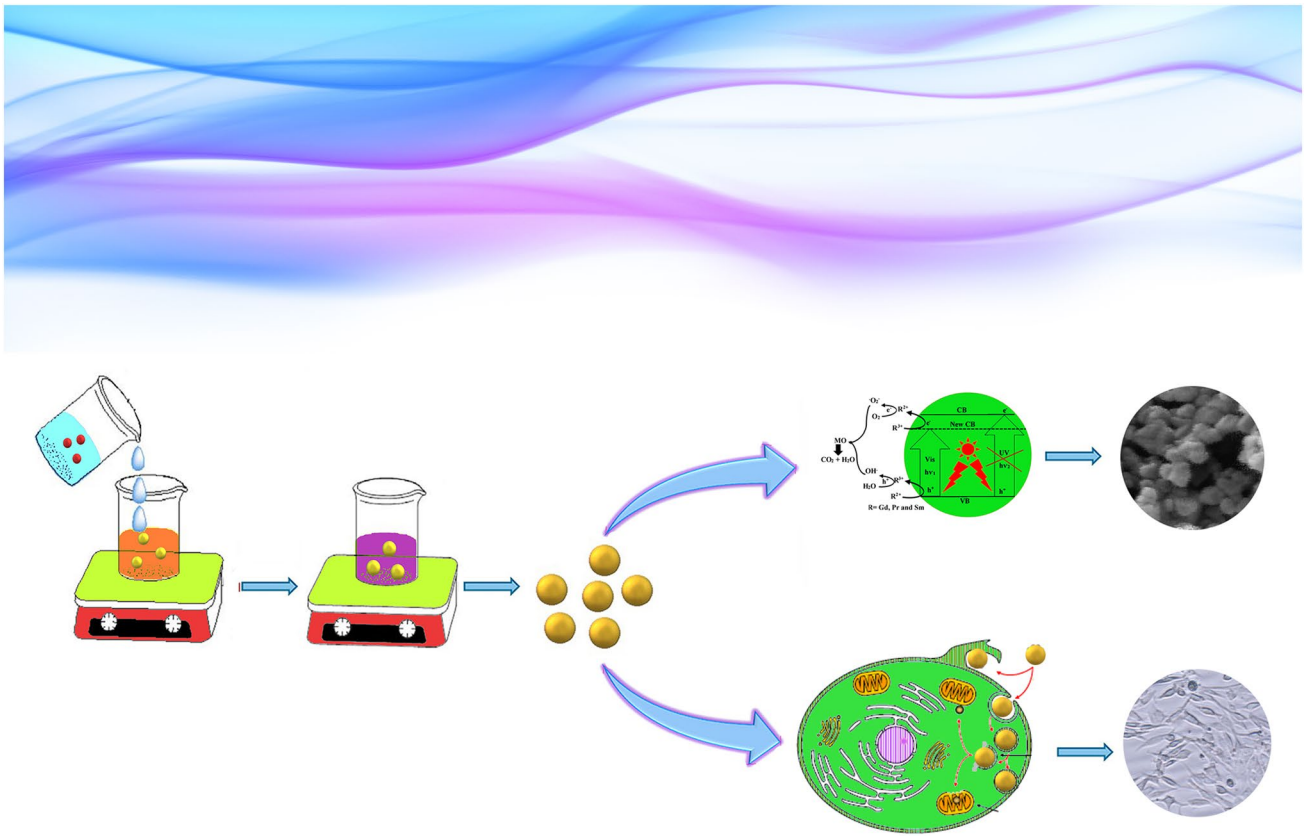

Scheme 1 Schematic depiction for the preparation of nanoparticles and its application in photocatalysts and Anti-cancer

at lower concentrations (250 µg/mL or lower). But after 48 h of cellular treatment with synthesized nanoparticles, some changes in the level of cytotoxicity were observed. As the $Li_{0.5}Fe_{2.5}O_4$ nanoparticles still showed no toxicity at a concentration of 500 µg/mL, the $LiMg_{0.5}Fe_2O_4$ and $LiNi_{0.5}Fe_2O_4$ nanoparticles destroyed 11% and 9% of the cells at this concentration respectively. However, at the concentration of 250 µg/mL, they did not have any toxicity. Synthesis pathway of the nanoparticles and their different applications is shown in Scheme 1. Figure 11 exhibits the microscopic photos of hela cells with optimized nanocomposite at three different concentrations which confirm that once concentrations decrease, the toxicity of the sample is reduced as well.

4 Conclusion

In summary, the obtained results demonstrate that the Ni (99.09%) or Mg-doped (98.04%) $Li_{0.5}Fe_{2.5}O_4$ has higher photoactivity in decomposition of MO under UV light illumination as compared with $Li_{0.5}Fe_{2.5}O_4$ nanoparticles (95%) which were directly synthesized through a facile sol–gel auto-combustion (SGAC) method. The XRD result shows that the average nanophotocatalyst samples was ~ 80 – 140 nm calculated by Debye–Scherrer formula. The approximately agglomerated nanophotocatalyst samples with average diameter sizes ranging from 90 to 205 nm were obtained via SEM technique. The $Li_{0.5}Fe_{2.5}O_4$ nanophotocatalysts display typical ferrimagnetic properties with

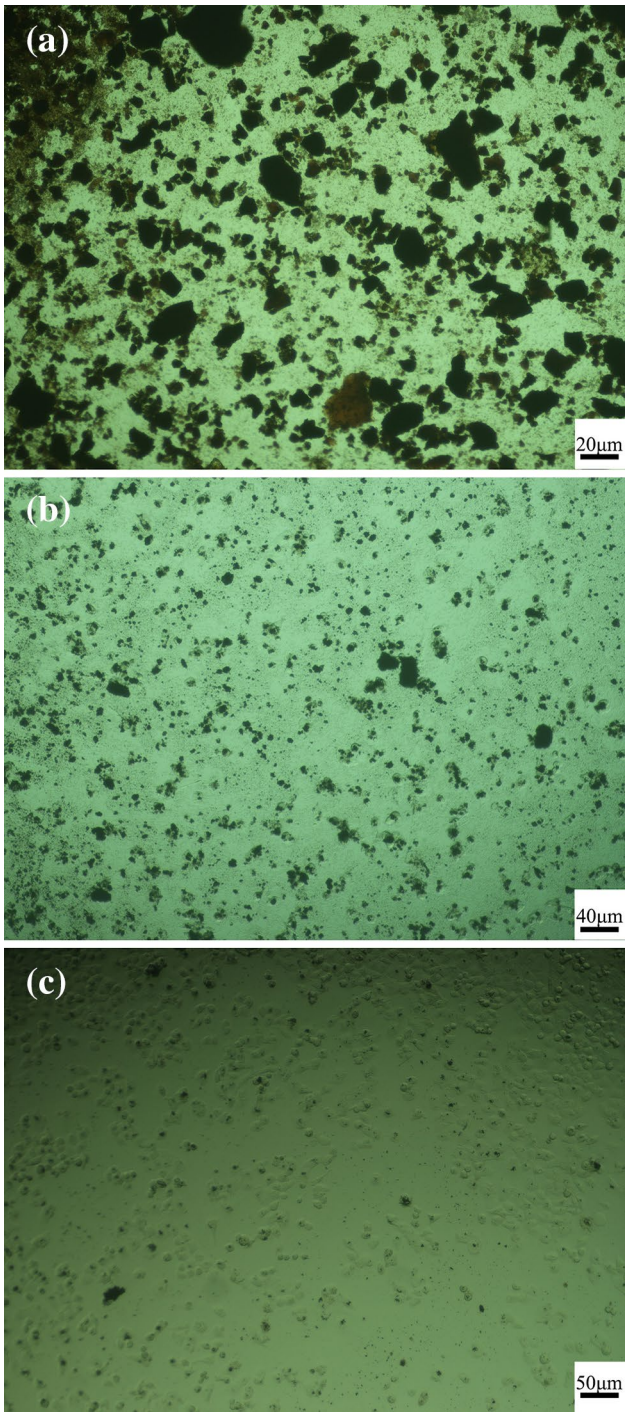

Fig. 11 Microscopic photograph of hela cell in the presence of nanocomposite specimen at three concentrations (**a**) 2, (**b**) 0.5, and (**c**) 0.0157 mg/mL

a maximum M_s of 57.757 emu/g. The band gap energy of $Li_{0.5}Fe_{2.5}O_4$ is decrease with doping Ni or Mg. Therefore the $Li_{0.5}Fe_{2.5}O_4$ nanoparticles still showed no toxicity at a concentration of 500 μg/mL while the $LiMg_{0.5}Fe_2O_4$ and $LiNi_{0.5}Fe_2O_4$ nanoparticles destroyed 11% and 9% of the cells at this concentration respectively. Meanwhile, at the concentration of 250 μg/mL, they did not have any toxicity.

Funding Funding was supported by Baqiyatallah University of Medical Sciences (Grant No. 942323).

References

1. M. Rostami, R.M. Zamani, K.M. Aghajanzadeh, H. Danafar, Sol–gel synthesis and characterization of zinc ferrite–graphene nano-hybrids for photo-catalytic degradation of the paracetamol. J. Pharm. Investig. (2017). https://doi.org/10.1007/s40005-017-0362-4
2. F. Ahmadi, M. Rahimi-Nasrabadi, M. Behpour, Synthesis Nd_2TiO_5 nanoparticles with different morphologies by novel approach and its photocatalyst application. J. Mater. Sci. Mater. Electron. **28**, 1531–1536 (2017)
3. M.A. Marsooli, M. Fasihi-Ramandi, K. Adib, S. Pourmasoud, F. Ahmadi, M.R. Ganjali, A. Sobhani Nasab, M.R. Nasrabadi, M.E. Plonska-Brzezinska. Preparation and Characterization of Magnetic $Fe_3O_4/CdWO_4$ and $Fe_3O_4/CdWO_4/PrVO_4$ Nanoparticles and Investigation of Their Photocatalytic and Anticancer Properties on PANC1 Cells. Materials. **12**(19) 3274 (2019)
4. M. Rahimi-Nasrabadi, F. Ahmadi, M. Eghbali-Arani, Simple morphology-controlled fabrication of $CdTiO_3$ nanoparticles with the aid of different capping agents. J. Mater. Sci.: Mater. Electron. **27**, 13294–13299 (2016)
5. A. Sobhani-Nasab, S. Behvandi, M.A. Karimi, E. Sohouli, M.S. Karimi, N. Gholipour, F. Ahmadi, M. Rahimi-Nasrabadi, Synergetic effect of graphene oxide and C3N4 as co-catalyst for enhanced photocatalytic performance of dyes on $Yb_2(MoO_4)$ 3/$YbMoO_4$ nanocomposite. Ceramics International. **45**(14), 17847–17858 (2019)
6. A. Sobhani-Nasab, S.M. Hosseinpour-Mashkani, M. Salavati-Niasari, H. Taqriri, S. Bagheri, K. Saberyan, Synthesis, characterization, and photovoltaic application of $NiTiO_3$ nanostructures via two-step sol–gel method. J. Mater. Sci.: Mater. Electron. **26**, 5735–5742 (2015)
7. A. Sobhani-Nasab, M. Behpour, M. Rahimi-Nasrabadi, F. Ahmadi, S. Pourmasoud, New method for synthesis of $BaFe_{12}O_{19}/Sm_2Ti_2O_7$ and $BaFe_{12}O_{19}/Sm_2Ti_2O_7$/Ag nano-hybrid and investigation of optical and photocatalytic properties. J. Mater. Sci.: Mater. Electron. **30**(6), 5854–5865 (2019)
8. S.M. Peymani-Motlagh, A. Sobhani-Nasab, M. Rostami, H. Sobati, M. Eghbali-Arani, M. Fasihi-Ramandi, M.R. Ganjali, M. Rahimi-Nasrabadi, Assessing the magnetic, cytotoxic and photocatalytic influence of incorporating Yb^{3+} or Pr^{3+} ions in cobalt nickel ferrite. J. Mater. Sci.: Mater. Electron. **30**(7), 6902–6909 (2019)
9. F. Sedighi, M. Esmaeili-Zare, A. Sobhani-Nasab, M. Behpour, Synthesis and characterization of $CuWO_4$ nanoparticle and $CuWO_4$/NiO nanocomposite using co-precipitation method; application in photodegradation of organic dye in water. J. Mater. Sci.: Mater. Electron. **29**, 13737–13745 (2018)
10. M. Eghbali-Arani, A. Sobhani-Nasab, M. Rahimi-Nasrabadi, S. Pourmasoud, Green synthesis and characterization of $SmVO_4$ nanoparticles in the presence of carbohydrates as capping agents with investigation of visible-light photocatalytic properties. J. Electron. Mater. **47**(7), 3757–3769 (2018)
11. S.M. Pourmortazavi, M. Rahimi-Nasrabadi, A. Sobhani-Nasab, M. Sadeghpour Karimi, M.R. Ganjali, S. Mirsadeghi, Electrochemical synthesis of copper carbonates nanoparticles through

experimental design and the subsequent thermal decomposition to copper oxide. Mater. Res. Express **6**, 045065 (2019)
12. M. Rahimi-Nasrabadi, A. Ghaderi, H.R. Banafshe, M. Eghbali-Arani, M. Akbari, S. Pourmasoud, A. Sobhani-Nasab, Preparation of Co_2TiO_4 /$CoTiO_3$/Polyaniline ternary nano-hybrids for enhanced destruction of agriculture poison and organic dyes under visible-light irradiation. J. Mater. Sci. Mater. Electron. **30**, 15854–15868 (2019)
13. M. Rahimi-Nasrabadi, M. Behpour, A. Sobhani-Nasab, M.R. Jeddy, Nanocrystalline Ce-doped copper ferrite: synthesis, characterization, and its photocatalyst application. J. Mater. Sci.: Mater. Electron. **27**, 11691–11697 (2016)
14. M.A. Gabal, R.M. El-Shishtawy, Y.M. Al Angari, Structural and magnetic properties of nano-crystalline Ni–Zn ferrites synthesized using egg-white precursor. J. Magn. Magn. Mater. **324**, 879–2264 (2012)
15. H.M. Widatallah, C. Johnson, A.M. Gismelseed, I.A. Al-Omari, S.J. Stewart, S.H. Al-Harthi, S. Thomas, H. Sitepu, Structural and magnetic studies of nanocrystalline Mg-doped $Li_{0.5}Fe_{2.5}O_4$ particles prepared by mechanical milling. J. Phys. D Appl. Phys. **41**, 165006 (2008)
16. M. George, S.S. Nair, A.M. John, P.A. Joy, M.R. Anantharaman, Structural, magnetic and electrical properties of the sol-gel prepared $Li_{0.5}Fe_{2.5}O_4$ fine particles. J. Phys. D Appl. Phys. **39**, 900–910 (2006)
17. H. Zeng, T. Tao, Y. Wu, W. Qi, C. Kuang, S. Zhou, Y. Chen, Lithium ferrite ($Li_{0.5}Fe_{2.5}O_4$) nanoparticles as anodes for lithium ion batteries. RSC Adv. **4**, 23145–23148 (2014)
18. V. Sepelak, Nanocrystalline materials prepared by homogeneous and heterogeneous mechanochemical reactions (Matériaux nanocristallins obtenus grâce à des réactions dactivation mécanique homogènes et hétérogènes). Ann. Chim. Sci. Mater. **27**, 61–76 (2002)
19. H.W. Wang, S.C. Kung, Crystallization of nanosized Ni–Zn ferrite powders prepared by hydrothermal method. J. Magn. Magn. Mater. **270**, 230–236 (2004)
20. S.M. Asgarian, S. Pourmasoud, Z. Kargar, A. Sobhani-Nasab, M. Eghbali-Arani, Investigation of positron annihilation lifetime and magnetic properties of $Co_{1-x}Cu_xFe_2O_4$ nanoparticles. Mater. Res. Express **6**, 15023 (2019)
21. A. Sobhani-Nasab, S. Pourmasoud, F. Ahmadi, M. Wysokowskid, T. Jesionowski, H. Ehrlich, M. Rahimi-Nasrabadi, Synthesis and characterization of $MnWO_4$/$TmVO_4$ ternary nano-hybrids by an ultrasonic method for enhanced photocatalytic activity in the degradation of organic dyes. Mater. Lett. **238**, 159–162 (2019)
22. H. Kooshki, A. Sobhani-Nasab, M. Eghbali-Aranic, F. Ahmadi, V. Ameri, M. Rahimi-Nasrabadi, Eco-friendly synthesis of $PbTiO_3$ nanoparticles and $PbTiO_3$/carbon quantum dots binary nanohybrids for enhanced photocatalytic performance under visible light. Sep. Purif. Technol. **18**, 873–878 (2019)
23. S. Kar, R.K. Choubey, P. Sen, G. Bhagavannarayana, K.S. Bartwal, Studies on codoping behavior of Nd:mg:$LiNbO_3$ crystals. Physica B Condens. Matter **393**(1–2), 37–42 (2007)
24. S. Kumar, A. Jain, S. Panwar, I. Sharma, H.C. Jeon, T.W. Kang, R.K. Choubey, Effect of silica on the ZnS nanoparticles for stable and sustainable antibacterial application. Int. J. Appl. Ceram. Technol. **16**(2), 531–540 (2019)
25. S. Kumar, T.W. Kang, S.J. Lee, S. Yuldashev, S. Taneja, S. Banyal, M. Singhal, G. Ghodake, H.C. Jeon, D.Y. Kim, R.K. Choubey, Correlation of antibacterial and time resolved photoluminescence studies using bio-reduced silver nanoparticles conjugated with fluorescent quantum dots as a biomarker. J. Mater. Sci.: Mater. Electron. **30**(7), 6977–6983 (2019)
26. S.E. Shirsath, R.H. Kadam, A.S. Gaikwad, A. Ghasemi, A. Morisako, Effect of sintering temperature and the particle size on the structural and magnetic properties of nanocrystalline $Li_{0.5}Fe_{2.5}O_4$. J. Magn. Magn. Mater. **323**, 3104–3108 (2011)
27. C. Cannas, A. Musinu, D. Peddis, G. Piccaluga, Synthesis and characterization of $CoFe_2O_4$ nanoparticles dispersed in a silica matrix by a sol–gel autocombustion method. Chem. Mater. **18**, 3835–3842 (2006)
28. X.Y. Li, Y. Hou, Q.D. Zhao, L.Z. Wang, A general, one-step and template-free synthesis of sphere-like zinc ferrite nanostructures with enhanced photocatalytic activity for dye degradation. J. Colloid Interf. Sci. **358**, 102–108 (2011)
29. A. Ahniyaz, T. Fujiwara, S.W. Song, M. Yoshimura, Low temperature preparation of β-$LiFe_5O_8$ fine particles by hydrothermal ball milling. Solid State Ionics **151**, 419–423 (2002)
30. Y. Sakurai, H. Arai, J. Yamaki, Preparation of electrochemically active α-$LiFeO_2$ at low temperature. Solid State Ionics **113**, 29–34 (1998)
31. M. Rahimi-Nasrabadi, M. Behpour, A. Sobhani-Nasab, S. Hosseinpour-Mashkani, $ZnFe_{2-x}La_xO_4$ nanostructure: synthesis, characterization, and its magnetic properties. J. Mater. Sci.: Mater. Electron. **26**, 9776–9781 (2015)
32. A. Sobhani-Nasab, H. Naderi, M. Rahimi-Nasrabadi, M.R. Ganjali, Evaluation of supercapacitive behavior of samarium tungstate nanoparticles synthesized via sonochemical method. J. Mater. Sci.: Mater. Electron. **28**, 8588–8595 (2017)
33. A. Sobhani-Nasab, M. Sadeghi, Preparation and characterization of calcium tungstate nanoparticles with the aid of amino acids and investigation its photocatalytic application. J. Mater. Sci.: Mater. Electron. **27**, 7933–7938 (2016)
34. H.R Naderi, A. Sobhani-Nasab, M. Rahimi-Nasrabadi, M.R. Ganjali, Decoration of Nitrogen-doped Reduced Graphene Oxide with Cobalt Tungstate Nanoparticles for Use in High-Performance Supercapacitors. Appl. Surf. Sci. **423**, 1025–1034 (2017)
35. S.M. Hosseinpour-Mashkani, M. Maddahfar, A. Sobhani-Nasab, Precipitation synthesis, characterization, morphological control, and photocatalyst application of $ZnWO_4$ nanoparticles. J. Electron. Mater. **45**, 3612–3620 (2016)
36. S.M. Hosseinpour-Mashkani, M. Maddahfar, A. Sobhani-Nasab, Novel silver-doped $CdMoO_4$: synthesis, characterization, and its photocatalytic performance for methyl orange degradation through the sonochemical method. J. Mater. Sci.: Mater. Electron. **27**, 474–480 (2016)
37. M. Rahimi-Nasrabadi, S.M. Pourmortazavi, M.R. Ganjali, P. Norouzi, F. Faridbod, M. Sadeghpour Karimi, Statistically optimized synthesis of dyspersium tungstate nanoparticles as photocatalyst. J. Mater. Sci. Mater. Electron. **27**, 12860–12868 (2016).
38. A. Khoshroo, L. Hosseinzadeh, A. Sobhani-Nasab, M. Rahimi-Nasrabadi, H. Ehrlich, Development of electrochemical sensor for sensitive determination of oxazepam based on silver-platinum core–shell nanoparticles supported on grapheme. J. Electroanal. Chem. **823**, 61–66 (2018)
39. M. Srivastava, A.K. Ojha, S. Chaubey, P.K. Sharma, A.C. Pandey, Influence of pH on structural morphology and magnetic properties of ordered phase cobalt doped lithium ferrites nanoparticles synthesized by sol–gel method. Mater. Sci. Eng., B **175**, 14–21 (2010)
40. M. Rahimi-Nasrabadi, M. Rostami, F. Ahmadi, A. Fallah Shojaei, M. Delavar Rafiee, Synthesis and characterization of $ZnFe_{2-x}Yb_xO_4$–graphene nanocomposites by sol–gel method. J. Mater. Sci.: Mater. Electron. **27**, 11940–11945 (2016)
41. A. Manikandan, J. Judith Vijaya, L. John Kennedy, M. Bououdina, Structural, optical and magnetic properties of $Zn_{1-x}Cu_xFe_2O_4$ nanoparticles prepared by microwave combustion method. J. Mol. Struct. **1035**, 332–340 (2013)
42. A.V. Dijken, E.A. Meulenkamp, D. Vanmaekelbergh, A. Meijerink, Identification of the transition responsible for the visible

emission in ZnO using quantum size effects. J. Lumin. **90**, 123–128 (2000)
43. M. Rostami, M. Rahimi-Nasrabadi, M.R. Ganjali, F. Ahmadi, A. Fallah Shojaei, M. Delavar Rafiee, Facile synthesis and characterization of TiO_2–graphene–$ZnFe_{2-x}Tb_xO_4$ ternary nano-hybrids. J. Mater. Sci. **52**, 7008–7016 (2017)
44. J. Jing, L. Liangchao, X. Feng, Structural analysis and magnetic properties of Gd-doped Li-Ni ferrites prepared using rheological phase reaction method. J. Rare Earths **25**, 79–83 (2007)
45. M. Rahimi-Nasrabadi, S.M. Pourmortazavi, M. Aghazadeh, M.R. Ganjali, M. Sadeghpour Karimi, P. Novrouzi, Optimizing the procedure for the synthesis of nanoscale gadolinium(III) tungstate as efficient photocatalyst. J. Mater. Sci. Mater. Electron. **28**, 3780–3788 (2017)
46. Y. Li, X. Li, J. Li, J. Yin, Photocatalytic degradation of methyl orange by TiO_2 coated activated carbon and kinetic study. Water Res. **40**, 1119–1126 (2006)
47. S.M. Hosseinpour-Mashkani, A. Sobhani-Nasab, Green synthesis and characterization of $NaEuTi_2O_6$ nanoparticles and its photocatalyst application. J. Mater. Sci.: Mater. Electron. **28**, 4345–4350 (2017)
48. M. Rahimi-Nasrabadi, A. Ghaderi, H.R. Banafshe, M. Eghbali-Arani, M, Akbari, F. Ahmadi, S. Pourmasoud, A. Sobhani-Nasab. Preparation of Co_2 TiO_4/$CoTiO_3$/Polyaniline ternary nano-hybrids for enhanced destruction of agriculture poison and organic dyes under visible-light irradiation. J. Mater. Sci.: Mater. Electron. **30**(6), 5854–5865 (2019)
49. A. Sobhani-Nasab, M. Behpour, Synthesis and characterization of AgO nanostructures by precipitation method and its photocatalyst application. J. Mater. Sci.: Mater. Electron. **27**, 1191–1196 (2016)
50. S.M. Hosseinpour-Mashkani, A. Sobhani-Nasab, Simple synthesis and characterization of copper tungstate nanoparticles: investigation of surfactant effect and its photocatalyst application. J. Mater. Sci.: Mater. Electron. **27**(7), 7548–7553 (2016)
51. M. Maddahfar, M. Ramezani, M. Sadeghi, A. Sobhani-Nasab, NiAl2O4 nanoparticles: synthesis and characterization through modify sol–gel method and its photocatalyst application. J. Mater. Sci. Mater. Electron. **26**, 7745–7750 (2015)
52. M. Ramezani, S.M. Hosseinpour-Mashkani, A. Sobhani-Nasab, H.G. Estarki, Synthesis, characterization, and morphological control of $ZnMoO_4$ nanostructures through precipitation method and its photocatalyst application. J. Mater. Sci.: Mater. Electron. **26**, 7588–7594 (2015)
53. M. Ramezani, A. Sobhani-Nasab, S.M. Hosseinpour-Mashkani, Synthesis, characterization, and morphological control of $Na_{1/2}Bi_{1/2}Cu_3Ti_4O_{12}$ through modify sol–gel method. J. Mater. Sci.: Mater. Electron. **26**, 4848–4853 (2015)
54. H. Eskandarloo, A. Badiei, M.A. Behnajady, G.M. Ziarani, Photo and chemical reduction of copper onto anatase-type TiO_2 nanoparticles with enhanced surface hydroxyl groups as efficient visible light photocatalysts. Photochem. Photobiol. **9**, 797–806 (2015)